J Therm Anal Calorim (2011) 105:883–896
DOI 10.1007/s10973-011-1464-2

Analyzing the calcination of sulfur-rich calcareous oil shales using FT-IR spectroscopy and applying curve-fitting technique

Shlomo Shoval · Yaacov Nathan

ESTAC2010 Conference Special Issue

Abstract The thermal processes during progressive calcination of sulfur-rich calcareous oil shales were analyzed using FT-IR spectroscopy and applying curve-fitting technique. The spectroscopic analysis is advantageous in the analysis of amorphous and short-range ordered thermal phases lacking of XRD peaks. The raw calcareous oil shales are composed of organic matter, kaolinite, smectite, calcite, and apatite (francolite). The principal thermal phases are metakaolinite, meta-smectite, free lime, anhydrite, gehlenite, and ellestadite. The thermal reactions observed with increase temperatures includes decomposition of organic matter followed by release of sulfur gas; dehydroxylation of kaolinite; and smectite at 500–600 °C; and thermal transformation to metakaolinite and meta-smectite; decarbonation of microcrystalline calcite to free lime at 600 °C; reaction of the sulfur gas with the free lime; formation of anhydrite at 600 °C; reaction of apatite and formation of ellestadite at 800 °C; reaction of the metakaolinite; the meta-smectite with the free lime; formation of gehlenite at 900 °C. Owingto the sulfatization process, a great part of the sulfur content of the raw oil shales is retained in the calcined ashes and the release of sulfur gas to the atmosphere decreases. Thus, the combustion of calcareous oil shales for energy source has less pollution effect than that of the clayey oil shales. FT-IR spectroscopy and spectral analysis seems to be useful methods for phase analysis of oil shales in combustion industry.

Keywords Anhydrite · Combustion · Ellestadite · Environmental · FT-IR spectroscopy · Gehlenite · Metakaolinite · Meta-smectite Oil shale · Sulfatization

S. Shoval (✉)
Geology Group, Department of Natural Sciences, The Open University of Israel, The Dorothy de Rothschild Campus, 1 University Road, Raanana, Israel
e-mail: shovals@openu.ac.il

Y. Nathan
Department of Geochemistry and Environmental Studies, The Geological Survey of Israel, 30 Malkhei Israel St., 90550 Jerusalem, Israel

Introduction

Oil shale deposits are an alternative source of fossil fuels. Their use becomes more attractive because of their abundance and the depletion of other natural energy resources. However, sulfur-rich oil shales may contain sulfur as much as 7% [1, 2], and their combustion has pollution effect on the environmental due to the release of sulfur gas to the atmosphere. In addition, their combustion left over large amounts of ash that contain heavy metals [3]. In the present study, the calcination of sulfur-rich calcareous oil shales from the Negev deposits of Israel is investigated. The Negev oil shales naturally contain a large amount of calcite, which may functioned as a sulfur-removing adsorbent. Therefore, the study of their calcination is of interest.

The Negev oil shales are organic-rich deposits from the Upper Cretaceous. These deposits have been traditionally termed "oil shales" although their lithology is in fact organic-rich marl [4]. The mineral composition of the Maastrichtian oil shales (Ghareb Formation) consists of calcite (50–60%), clays (2–25%), apatite (2–10%), and quartz (2–6%) [5]. The dominant clay mineral is kaolinite, with minor amounts of montmorillonite and illite. Other minerals are dolomite (<5%) gypsum (<5%), and pyrite (<2%). The total organic carbon concentration usually ranges up to 17%, and the principal organic compounds are

kerogens and some bitumens [6]. The amount of sulfur in these oil shales appears up to 5%.

The calcareous oil shales of the Negev are utilized in a demonstration power plant of the PAMA (Energy Resource Development Ltd) company [5, 7]. Their combustion takes place in a fluidized-bed reactor. Their mineral reactions and pyrolysis were studied by Heller-Kallai et al. [8]. During the combustion the organically bonded sulfur released during the pyrolysis reacts with oxygen from the fluidizing air and with free lime (CaO) resulting from the decarbonation of calcite to form anhydrite ($CaSO_4$). At pyrolysis and coke-oxidation temperature near 600 °C, kaolinite [$Al_2Si_2O_5(OH)_4$] reacts to form amorphous modified metakaolinite ($Al_2Si_2O_7$). At organic gas combustion temperature near 1,000 °C, the amorphous phases in the overhead fines react with additional calcite and quartz to form gehlenite ($Ca_2Al_2SiO_7$) and larnite (β-Ca_2SiO_4). In organic-rich oil shale the sulfatization process may also produce hydroxylellestadite [$Ca_{10}(SO_4, SiO_4,PO_4)_6(OH)_2$] [5, 7]. Formation of the latter mineral was also found in Japanese coal power plants when high-purity limestone was added for in-bed sulfur removal in pressurized fluidized-bed combustion [9].

In the present study, the thermal products that formed during the calcination of sulfur-rich calcareous oil shales from the Negev deposits were analyzed using FT-IR spectroscopy and curve-fitting technique. These techniques allow the identification of individual thermal phases [10].

Experimental

Samples

Organic-rich calcareous oil shales from the Negev deposits were collected in the Ein-Bokek deposit located in the Dead Sea region. The samples were taken from the Upper Cretaceous (Maastrichtian) Ghareb Formation. A list of the samples investigated is given in Table 1. Reference minerals of anhydrite, gehlenite, and ellestadite were taken from the OU collection.

Thermal treatment

The calcareous oil shales were heated in an electric kiln to temperature intervals ranging from 400 to 1,000 °C. The heating time was 6 h at each temperature interval, which is reasonable for the end of the indicative thermal reactions at defined temperature. The measurements were obtained at room temperature.

Methods

The samples were investigated by the following methods:

- *X-ray powder diffraction* (*XRD*): using acquired with a Philips PW-3710 diffractometer using Cu-Kα radiation 35 kV, 40 mA, and a curved graphite monochromator.
- *Infrared spectroscopy* (*FT-IR*): FT-IR spectra were obtained using Jasco-4100 FT-IR spectrometer and Spectra Manager software. The samples were examined in pressed KBr disks. Mixtures of 1 mg of the powdered sample and 150 mg of KBr were mixed by grinding in an agate mortar and pressed into disks. The disks were examined at room temperature and also immediately after heating to 110 °C to remove the absorbed water. Before measurement, the heated disks were repressed to improve the resolution of the spectra. Accumulations of 60 s were applied for the spectra collection.
- *Energy Dispersive Spectroscopy* (*EDS*): Chemical analyses of the raw and the calcined oil shales were obtained using LINK-10000 EDS (Oxford ISIS) attached to a JEOL (JSM-840) SEM instrument. The samples were examined on aluminum stub holders covered by a carbon film. Calculations were made using the ZAF4/FLS program. The reference standard for X-ray microanalysis of Microanalyses Consulted Ltd. (Registered standard 1691) was used for the EDS analysis. Accumulations of

Table 1 A list of the raw calcareous oil shales investigated, their mineral composition observed by XRD and the amounts of carbonate minerals and organic matter

Sample	Deposit	Mineral composition	Carbonate minerals/%	Organic matter/%
EB-1	Ein-Bokek	Do, Ka, Sm, Qu, Gy	25	15
EB-2	Ein-Bokek	Do, Ka, Sm, Ap, Qu	20	15
EB-3	Ein-Bokek	Ca, Do, Ka, Sm, Ap, Qu	45	10
EB-4	Ein-Bokek	Do, Ka, Sm, Ap, Qu	40	8
EB-5	Ein-Bokek	Ca, Do, Ka, Sm, Ap, Qu, Gy	45	10

Ap apatite, *Ca* calcite, *Do* dolomite, *Gy* gypsum, *Ka* kaolinite, *Qu* quartz, *Sm* smectite

60 s (3–5 iterations) were applied for the chemical analyses. The analytic error is ±2%.

– *Thermogravimetric analysis* (*TG and DTG*): was done by measuring the thermal weight-loss. The DTG curves were obtained using Origin software.

Results

The raw calcareous oil shales

X-ray diffraction

The mineral composition of the raw calcareous oil shales examined is demonstrated in Table 1. The oil shales consist of calcite or dolomite, kaolinite, smectite, quartz, apatite (francolite), and gypsum.

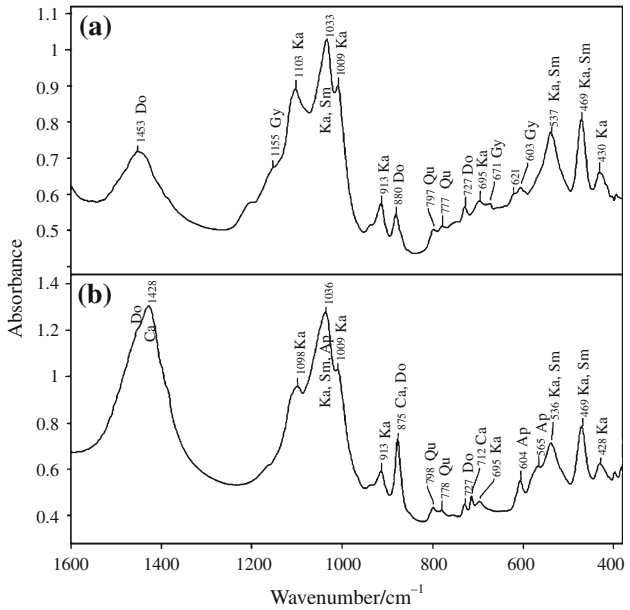

Fig. 1 FT-IR spectra of representative raw calcareous oil shales: **a** sample EB-1 (without apatite); and **b** sample EB-3 (with apatite). *Ap* apatite, *Ca* calcite, *Do* dolomite, *Gy* gypsum, *Ka* kaolinite, *Qu* quartz, and *Sm* smectite

FT-IR spectroscopy

FT-IR spectra of representative raw calcareous oil shales are demonstrated in Fig. 1. The mineral compositions of the raw calcareous oil shales were identified by their indicative bands in the infrared spectra [11]. The FT-IR results are in agreement with the XRD analyses. The locations of the CO_3 bands at 1,453 and 727 cm^{-1} are diagnostic of dolomite (Fig. 1a) and at 1,428 and 712 cm^{-1} are characteristic of calcite (Fig. 1b). The main band at about 1,033 and the band at 469 cm^{-1} are of clay minerals (mainly kaolinite). The band-doublet at about 778 and 798 cm^{-1} distinguish quartz (Fig. 1). The band at 603 cm^{-1} is diagnostic of gypsum (Fig. 1a), and the bands at 565 and 604 cm^{-1} are diagnostic of apatite (Fig. 1b). The main bands of the quartz at 1,084, the apatite at 1,042 cm^{-1}, and the gypsum at 1,120 and 1,150 cm^{-1} are distorted by the principal band of the clay. The results demonstrate that sample EB-1 is richer in clay (mainly kaolinite), and sample EB-3 contains some apatite.

Chemical analysis

The chemical composition of the raw calcareous oil shales is depicted in Table 2. The amounts of the oxides represent the content of the subsequent minerals: CO_3 the carbonate minerals and the organic matter; SiO_2—clays and quartz; Al_2O_3—clays; CaO—calcite, dolomite, some apatite, and some gypsum; P_2O_5—apatite; SO_3—organic matter, some gypsum and some pyrite; MgO—dolomite; FeO—iron oxides, TiO_2—some titanium minerals (anatase); K_2O—some K-feldspar; and Na_2O some salt (halite).

The thermally treated calcareous oil shales

X-ray diffraction

The mineral composition of the calcined calcareous oil shales after calcination at 600, 800, and 1000 °C are demonstrated in Table 3. XRD diffractograms of calcined calcareous oil shales heated to 1,000 °C are demonstrated in Fig. 2. The principal thermal phases observed in the diffractograms are free lime, anhydrite, gehlenite, and

Table 2 The major element composition (normalized to 100%) of the raw calcareous oil shale investigated

Sample	CO_3	SiO_2	Al_2O_3	CaO	P_2O_5	SO_3	MgO	FeO	TiO_2	K_2O	Na_2O
EB-1	63.8	7.9	4.0	4.0	1.0	5.6	5.6	1.1	0.0	1.4	5.6
EB-2	62.0	11.8	6.5	4.5	1.0	2.9	2.7	1.7	0.4	0.6	5.9
EB-3	60.1	10.3	5.1	14.2	2.5	2.5	2.5	1.2	0.2	0.5	0.8
EB-4	54.3	11.3	5.0	16.3	2.5	2.8	4.3	1.6	0.4	0.6	0.9
EB-5	56.5	10.7	5.2	16.1	1.5	3.7	2.9	1.6	0.2	0.6	0.9

Table 3 The mineral composition observed by XRD of the calcareous oil shales after calcination at 600, 800, and 1000 °C

Sample	600 °C	800 °C	1000 °C
EB-1	An, Li, Qu	Ap, Ge, Li, He	An, Ge, He
EB-2	An, Li, Ap, Qu	Ap–El, Ge, Li	Ap–El, Ge, Li
EB-3	An, Pr, Ap, Qu, Pr	Ap–El, Ge, Pr	Ap–El, Ge, Pr, He
EB-4	An, Li, Ap, Qu	Ap–El, Ge, Li	Ap–El, Ge, Li
EB-5	An, Li, Ap, Qu	Ap–El, Ge, Li	Ap–El, Ge, Li

An anhydrite, *Ap* apatite, *El* ellestadite, *Ge* gehlenite, *He* hematite, *Li* free lime, *Pr* periclase, *Qu* quartz

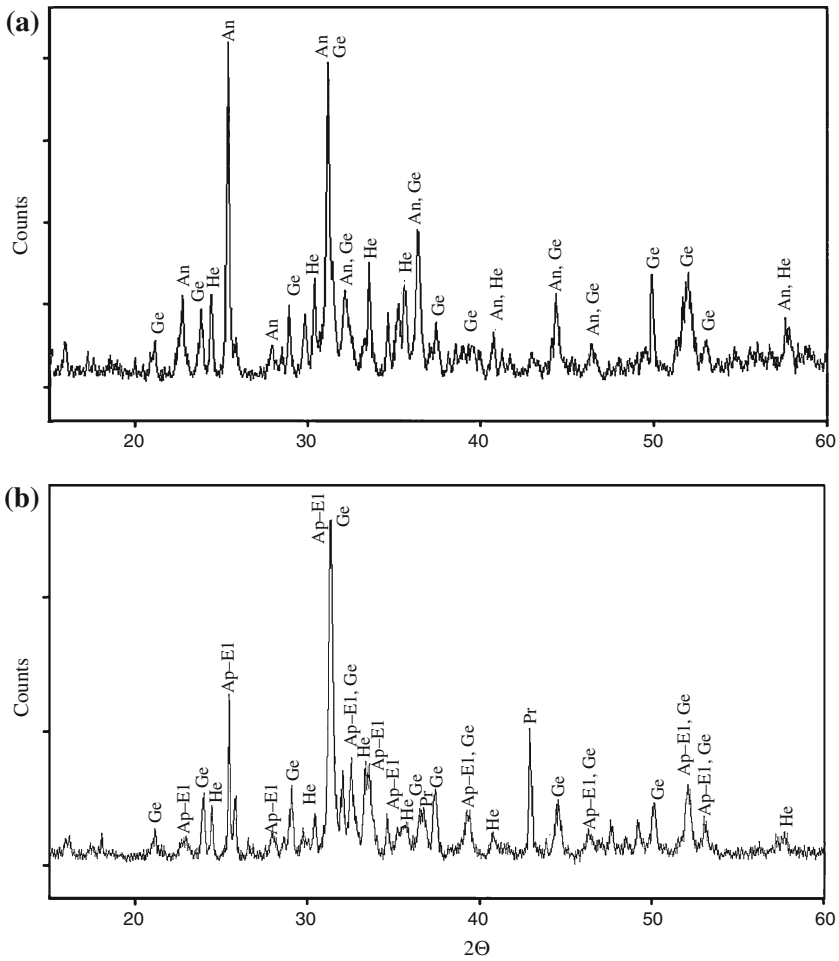

Fig. 2 XRD diffractograms of the calcined calcareous oil shales heated to 1,000 °C: **a** sample EB-1; and **b** sample EB-3. *An* anhydrite, *Ap* apatite, *El* ellestadite, *Ge* gehlenite, *He* hematite, *Pr* periclase

ellestadite. Apatite and ellestadite were not observed in the diffractogram of sample EB-1.

FT-IR spectroscopy

The different thermal products in the calcareous oil shales treated were identified according to the indicative bands in the infrared spectra. FT-IR spectra of standards of minerals typical for calcination of calcareous oil shales served as references for the identification. FT-IR spectra of the minerals anhydrite, gehlenite, and ellestadite are demonstrated in Fig. 3.

FT-IR spectra of representative calcined calcareous oil shales are demonstrated in Figs. 4, 5. The principal thermal phases observed in the spectra are metakaolinite, metasmectite, free lime, anhydrite, Ca-silicates, gehlenite, and ellestadite. Apatite and ellestadite were not observed in the spectrum of sample EB-1.

Curve-fitted FT-IR spectra

Curve-fitted FT-IR spectra of representative calcined calcareous oil shales are demonstrated in Figs. 6, 7. Frequencies of IR bands and their relative intensities are given

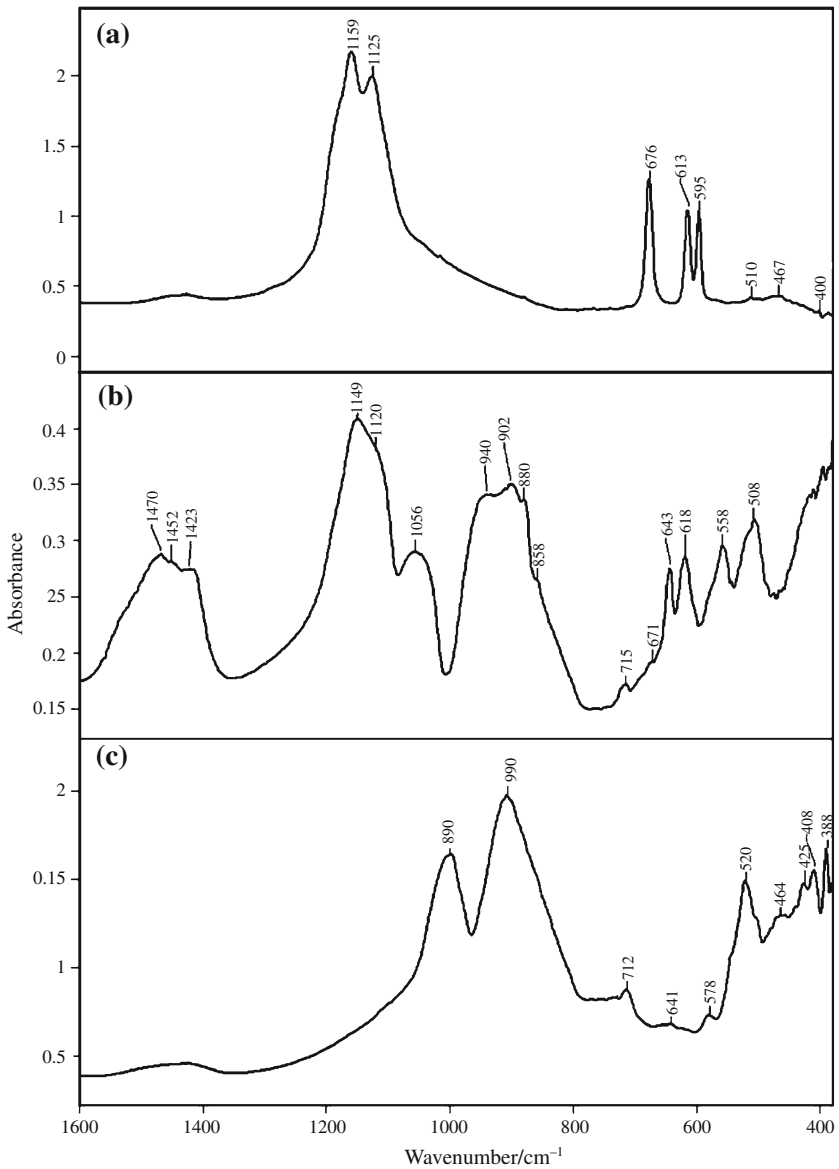

Fig. 3 FT-IR spectra of standards of minerals **a** anhydrite, **b** ellestadite, and **c** gehlenite, which served as references for the identification of the thermal phases in the calcined calcareous oil shales

in Tables 4, 5. The application of curve-fitting allows improving in the identification of the individual thermal phases and estimating their relative amounts. The peak fitting of the broad Si–O-stretching band enables to observed components of the thermal phases of metakaolinite, meta-smectite, and short-range-ordered thermal phases, which are lacking of XRD peaks. Table 4 shows the locations of the diagnostic components of the thermal phases in spectra recorded at different temperatures. Table 5 demonstrates the relative intensities of IR bands of the thermal phases at different heating temperatures. The relative band intensities give an indication on the relative amounts of the respective thermal phases.

FT-IR spectra in the range 4,000–2,600 cm^{-1} of the representative sample is demonstrated in Fig. 8. The sharp OH-stretching bands at 3620, 3652, and 3695 cm^{-1} are characteristic of kaolinite. The fourth kaolinite band at about 3,670 cm^{-1} appears as a very weak shoulder, indicating that the kaolinite is poorly ordered. The CH_2 and CH_3 bands at 2855, 2873, and 2927 cm^{-1} represent the organic matter.

The use of FT-IR spectroscopy enables us to observe the following changes during the progressive heating of the calcareous oil shales: At 400 °C: The spectra of the minerals are quite similar to those of the raw oil shales, but the CH_2 and CH_3 bands of the organic matter in the raw oil shales (Fig. 8a) decrease after calcination at 400 °C (Fig. 8b) because of thermal decomposition. At 600 °C: The OH stretching bands of the kaolinite in the raw oil shales (Fig. 8a), disappear after calcination at 600 °C (Fig. 8c) because of the thermal dehydroxylation and formation of metakaolinite. The main CO_3 bands of the

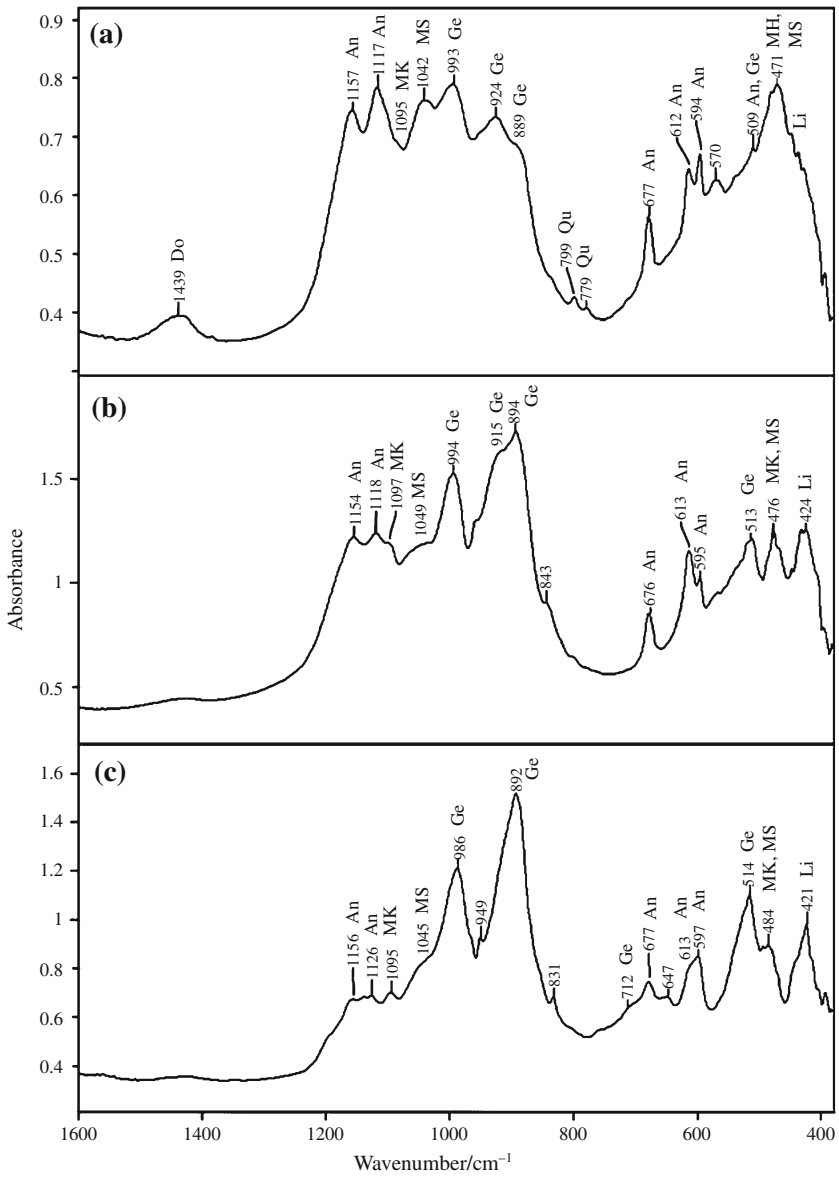

Fig. 4 FT-IR spectra of sample EB-1 after calcination at 600 (**a**), at 800 (**b**), and at 1,000 °C (**c**). *An* anhydrite, *Ap* apatite, *Do* dolomite, *Ge* gehlenite, *Li* free lime, *MK* metakaolinite, *MS* meta-smectite, and *Qu* quartz

dolomite and the calcite, which are located in the spectra of the raw oil shales at 1,453 (Fig. 1a) and at 1,428 cm^{-1} (Fig. 1b) almost disappears after calcination at 600 °C (Figs. 4a, 5a) because of the thermal decarbonation. As a result, free lime is formed as observed by the broad IR band at about 424 cm^{-1} (Figs. 4b, 5b). Periclase is also formed in samples containing dolomite. A remnant band-doublet of structural carbonate in apatite (francolite) is observed for the sample EB-3 at 1,424 and 1,456 cm^{-1} (Fig. 5a). Some anhydrite, ellestadite, and gehlenite are detected (Figs. 4, 5, 6, 7) by their diagnostic bands (Fig. 3). The amounts of the different thermal phases depend on the heating temperature (Table 5). Nevertheless, the variability in the amounts is related to the inhomogeneous composition of the natural samples and the contents of clay minerals and apatite.

Chemical analysis

The major element composition of the calcareous oil shales after calcination at 1,000 °C is shown in Table 6. The amounts of the oxides represent the content of the subsequent minerals at this temperature: SiO_2—meta-clays, quartz, gehlenite, and ellestadite; Al_2O_3—meta-clays and gehlenite; CaO—free lime, anhydrite, ellestadite, and gehlenite; P_2O_5—ellestadite; SO_3—anhydrite and ellestadite; MgO—periclase; FeO—hematite, TiO_2—some titanium minerals. K_2O—some K-feldspar; and Na_2O—some salt (halite). By comparing the amount of SO_3 in the oil shales heated to 1,000 °C to that of the raw oil shales (without the amount of CO_3), it appears that as a result of a sulfatization process, a great part of the SO_3 content of the raw oil shales is retained in the calcined ashes forming anhydrite and ellestadite.

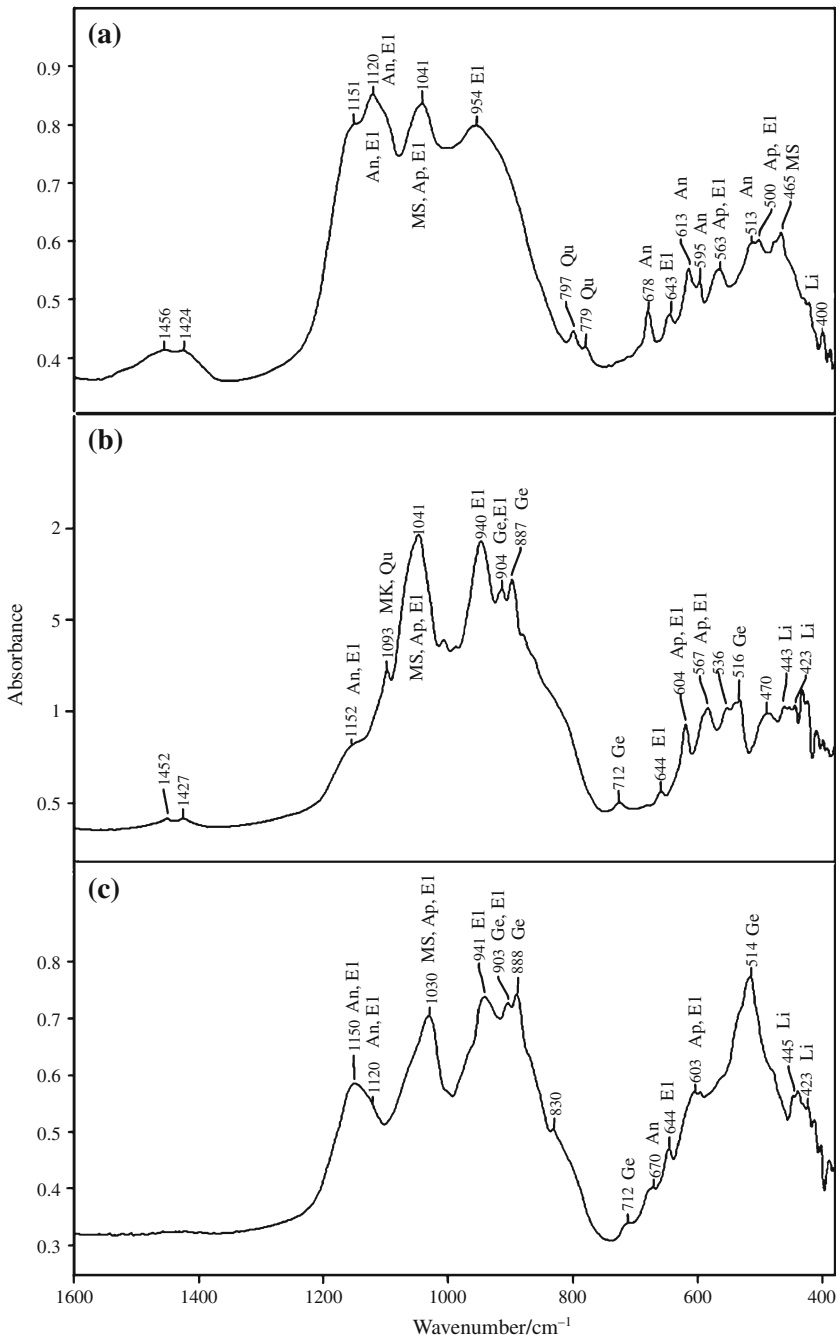

Fig. 5 FT-IR spectra of sample EB-3 after calcination at 600 (**a**), at 800 (**b**), and at 1,000 °C (**c**). *An* anhydrite, *Ap* apatite, *El* ellestadite, *Ge* gehlenite, *MK* metakaolinite, *MS* metasmectite, *Li* free lime, and *Qu* quartz

Thermal analysis

Thermogravimetric curves (TG and DTG) indicate the temperature in which the thermal reactions take place. The thermogravimetric curves of samples EB-3 and EB-5 are shown in Fig. 9. The peaks in the DTG curves are related to the dehydration of the water below 100 °C, decomposition of some organic matter at about 400 °C, dehydroxylation of clay minerals at about 500 °C, and decarbonation of carbonate minerals (calcite or dolomite) above 600 °C.

Discussion

The following thermal transformations were observed during the progressive heating of the calcareous oil shales (Fig. 9).

Decomposition of the organic matter

Decomposition of some organic matter is observed by the DTG curve (Fig. 9) and by the decrease of the CH_2, CH_3 bands in the spectra of the oil shales after heating at 400 °C

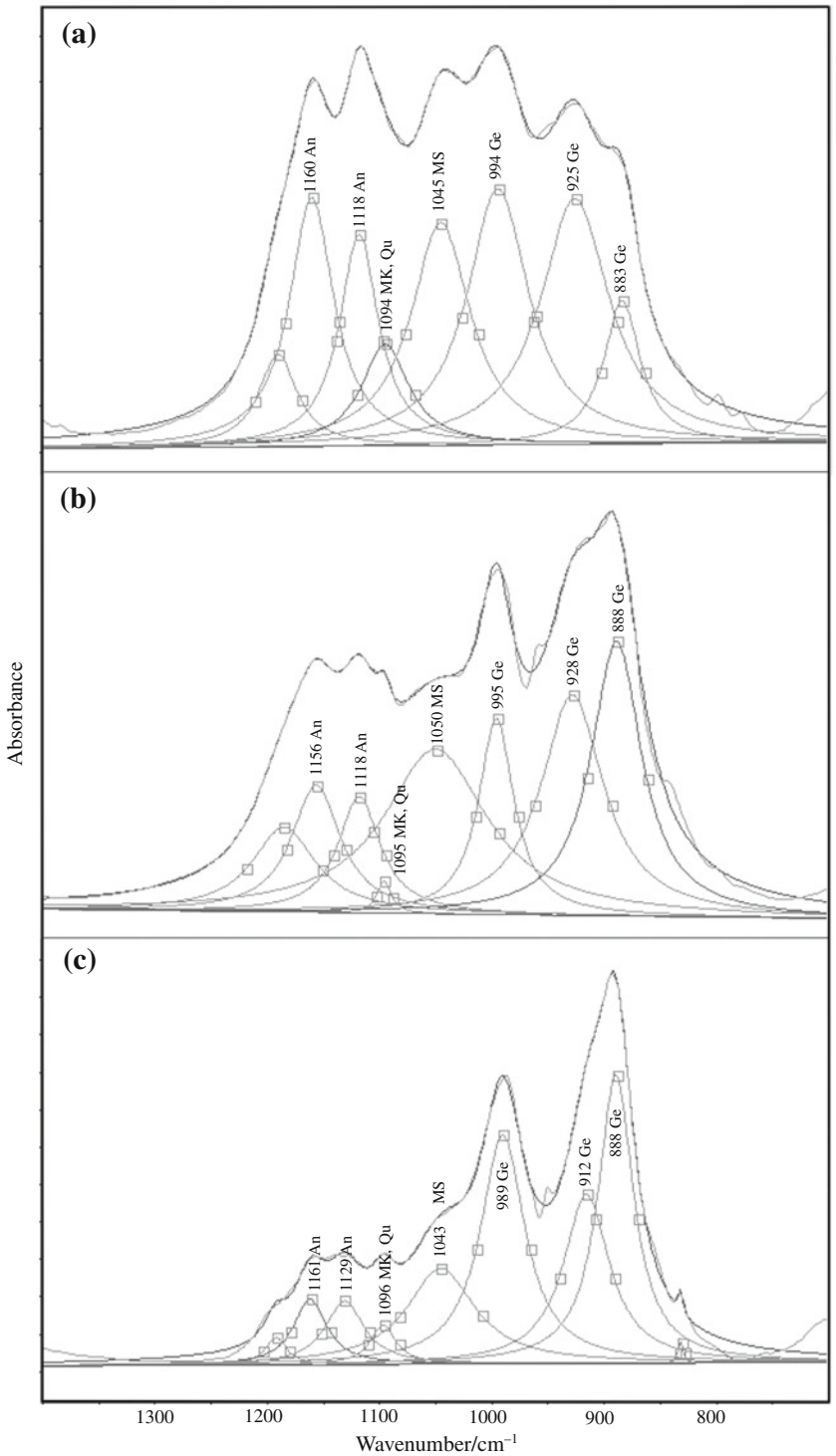

Fig. 6 Curve-fitted FT-IR spectra of sample EB-1 after calcination at 600 (**a**), at 800 (**b**), and at 1,000 °C (**c**). *An* anhydrite, *Ge* gehlenite, *MK* metakaolinite, *MS* metasmectite, and *Qu* quartz

(Fig. 8b). The decomposition of the organic matter brings about the separation of sulfur compounds followed by the release of sulfur gas. According to Heller-Kallai et al. [8], during pyrolysis of the oil shales at 550–650 °C, the organic polymer chain of the kerogen is broken more easily near the sulfur atoms. Sulfur dioxide (SO_2) is released because of oxidation of the sulfur separated by the decomposition of the organic matter. The thermal oxidation of the sulfur compounds and the sulfur dioxide (SO_2) at about 600 °C produces sulfur trioxide (SO_3).

Early decarbonation of the calcite

An early decarbonation of the calcite and the dolomite in the calcareous shales is observed by the DTG curve (Fig. 9) and by the almost disappearing CO_3 bands in the spectra of

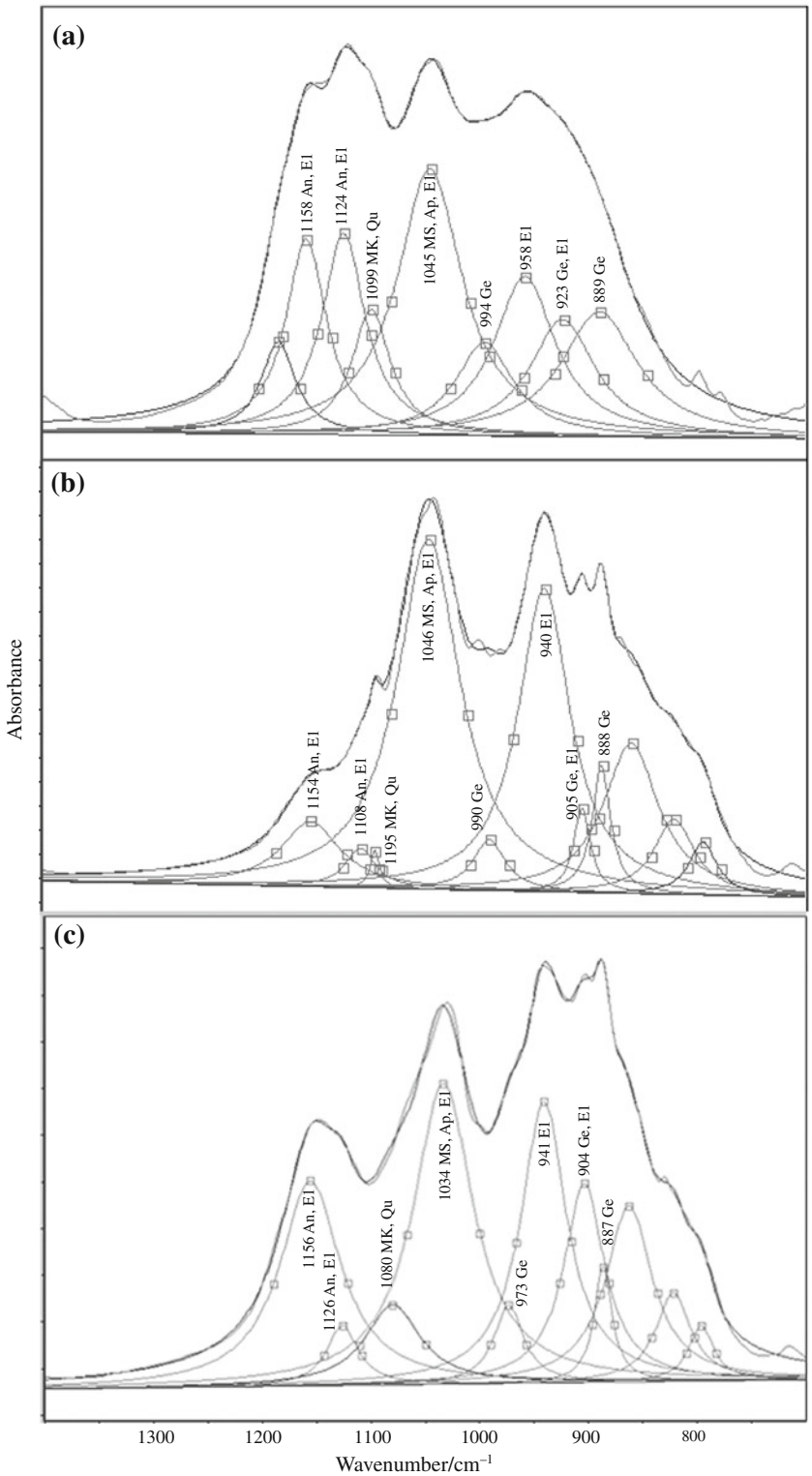

Fig. 7 Curve-fitted FT-IR spectra of sample EB-3 after calcination at 600 (**a**), at 800 (**b**), and at 1,000 °C (**c**). *An* anhydrite, *Ap* apatite, *El* ellestadite, *Ge* gehlenite, *MK* metakaolinite, *MS* metasmectite, and *Qu* quartz

samples heated at 600 °C (Figs. 4a, 5a). In this process, carbon dioxide gas (CO_2) is released from the calcite and free lime (CaO) is formed. In samples containing dolomite, periclase (MgO) is also formed. The decarbonation at about 600 °C is considered to be an early process—occurring at a lower temperature. The temperature of decarbonation depends on the duration of heating, the crystal size, the crystallinity of the original calcite, and the presence of impurities [12]. The presence of clay reduces the temperature of decarbonation [13–16]. It seems that in the

Table 4 Frequencies (cm^{-1}) of IR bands of the thermal phases in the curve fitted IR spectra of the calcined calcareous oil shales

Sample	Temperature/°C	An, El	An, El	MK, Qu	MS, Ap, El	Ge	El	Ge, El	Ge
EB-1	600	1160[a]	1118[a]	1094	1045[a]	994	[a]	925	883
	800	1156	1118	1095	1050	995	[a]	928	888
	1000	1161	1129	1096	1043	989	[a]	912	888
EB-2	600	1167	1118	1090	1043	1001	961	922	893
	800	1166	1138	1097	1042	994	950	915	886
	1000	1172	1148	1088	1039	997	956	908	878
EB-3	600	1158	1124	1099	1045	994	958	923	889
	800	1154	1108	1095	1046	990	940	905	888
	1000	1156	1126	1080	1034	973	941	904	887
EB-4	600	1157	1125	1100	1047	995	953	912	876
	800	1158	1116	1097	1045	990	940	895	886
	1000	1172	1147	1096	1032	980	939	912	887
EB-5	600	1169	1141	1104	1047	1002	954	913	883
	800	1162	1128	1099	1045	980	932	910	887
	1000	1157	1123	–	1035	978	938	905	887

[a] Apatite and ellestadite were not observed in sample EB-1

Table 5 Relative intensities of IR bands (in percentages) of the thermal phases in the curve fitted IR spectra of the calcined calcareous oil shales

Sample	Temperature/°C	An, El	An, El	MK, Qu	MS, Ap, El	Ge	El	Ge, El	Ge
EB-1	600	17.42[a]	14.84[a]	7.10	15.48[a]	18.06	[a]	17.42	9.68
	800	11.17	10.32	2.87	14.33	17.48	[a]	19.48	24.36
	1000	43.54	4.07	2.15	6.70	14.11	[a]	12.92	16.51
EB-2	600	14.97	16.04	9.09	29.41	16.04	6.95	4.28	3.21
	800	10.79	5.76	14.03	18.71	19.06	8.63	12.59	10.43
	1000	2.66	8.58	13.31	11.83	27.81	8.58	18.34	8.88
EB-3	600	15.24	15.85	9.76	20.73	7.32	12.20	9.15	9.76
	800	6.24	3.70	3.70	33.49	3.70	28.87	8.08	12.24
	1000	15.83	4.32	5.76	23.02	5.76	21.58	15.11	8.63
EB-4	600	8.62	9.48	9.48	23.28	6.90	20.26	11.21	10.78
	800	9.56	4.78	2.39	26.29	12.35	17.53	24.70	2.39
	1000	1.73	3.46	3.90	22.94	16.02	12.99	17.32	21.65
EB-5	600	5.43	5.43	16.28	27.13	6.98	26.36	6.98	5.43
	800	5.77	6.15	3.46	22.69	18.08	14.23	11.54	18.08
	1000	16.97	12.18	0.00	15.50	6.64	26.57	9.96	12.18

[a] Apatite and ellestadite were not observed in sample EB-1

calcination of the calcareous oil shales, the vapors released by the decomposition of the organic matter and by the dehydroxylation of the clay simulate the early decarbonation of the microcrystalline calcite composed these rocks [12–14]. Indeed, in the presence of clay, under prolonged heating (6 h), the decarbonation process is completed at about 600 °C in microcrystalline calcite (micrite) of chalk [12]. In contrast, large calcite crystals are decarbonated at a higher temperature, at about 800–900 °C. In DTA experiments, the endothermic peak of the decarbonation process of crystalline calcite appears only at about 900 °C [17] because of the rapid rate of heating and the higher crystallinity of the calcite.

In samples containing apatite, a weak band-doublet of a carbonate group is observed in the spectra at 600 °C, after removal of the bands of the calcite or the dolomite by the decarbonation (Fig. 5a). This band-doublet is related to structural carbonate in the apatite indicating that francolite (carbonate–fluorapatite) is present. The carbonate ion is expelled from the apatite structure at about 800 °C [18], as observed by the disappearance of the band-doublet of the carbonate group (Fig. 5c).

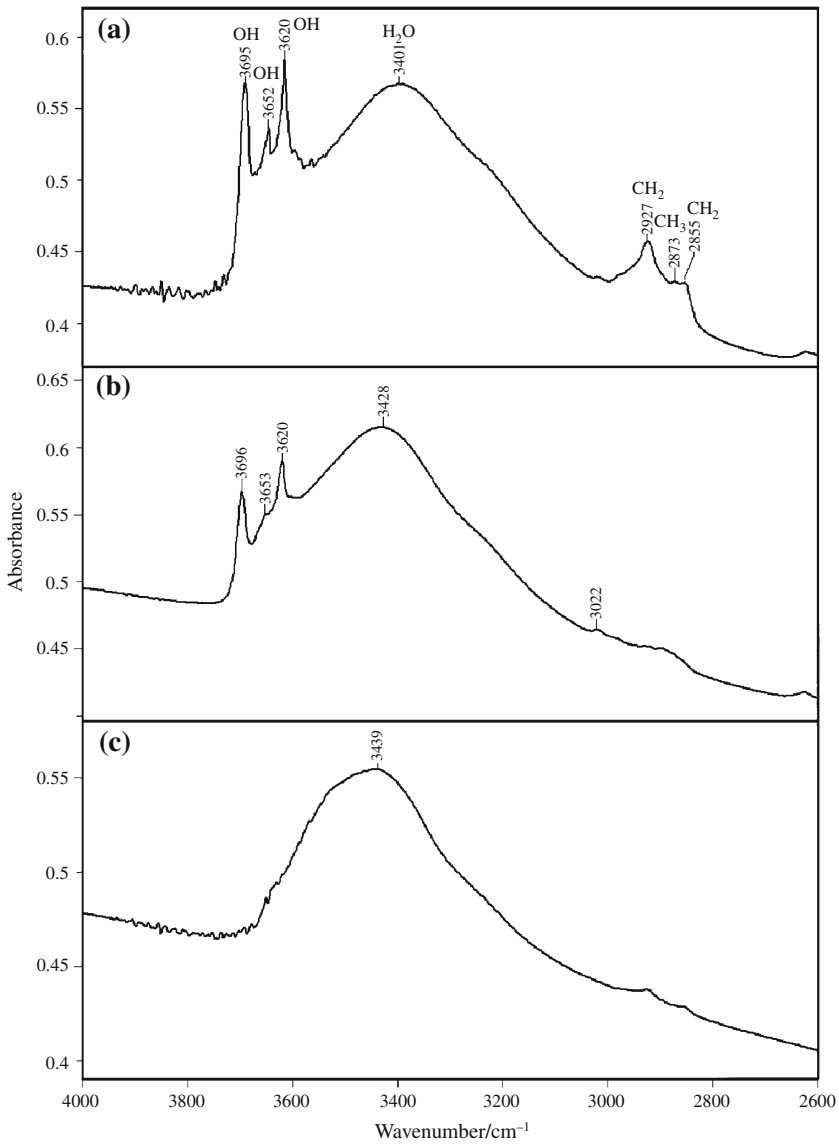

Fig. 8 FT-IR spectra in the range 4,000–2,600 cm^{-1} of the raw sample EB-3 (**a**) and after calcination at 400 (**b**), and at 600 °C (**c**). OH = OH-stretching bands in kaolinite, CH_2, and CH_3 = groups of organic matter

Thermal sulfatization process

Formation of thermal phase of anhydrite is observed in the spectra (Figs. 4a, 5a) and in the curve-fitted spectra (Figs. 6a, 7a) of samples heated at 600 °C. The formation of anhydrite in combustion oil shales by a thermal sulfatization process was reported by Heller-Kallai et al. and Nathan et al. [5, 7, 8]. The presence of gypsum and pyrite in the raw oil shales may have an additional source for the formation of anhydrite. Nevertheless, the amounts of gypsum and pyrite in the raw oil shales are less then 5 and 2%, respectively [19]. Indeed, in raw samples containing gypsum (Fig. 1a), the characteristic SO_4 bands of the gypsum have much less intensities than those of the anhydrite appearing at 600 °C (Figs. 4a, 6a), indicating that a greater part of the anhydrite is formed by the sulfatization process.

In the sulfatization process the SO_3, obtained from the decomposed organic matter, reacts with the free lime resulting from the decarbonation of calcite, and anhydrite is formed. It has been suggested that anhydrite is formed by reaction of SO_3 directly with calcite, without earlier decarbonation of the calcite [9, 20]. However, the present results demonstrate that free lime is formed at 600 °C, which is the temperature of the anhydrite formation. It therefore appears that the sulfatization process takes place by the reaction of SO_3 with the free lime.

Ellestadite is formed by this process in samples containing apatite (francolite, Figs. 5, 7). The term ellestadite is used here instead of hydroxylellestadite since the latter mineral is expected to be dehydroxylated at 800 °C. In addition, portlandite is formed in the calcined samples by the hydration of excess of free lime by picking up moisture from the air [21]. Thus, the sharp OH-stretching band at

Table 6 The major element composition (normalized to 100%) of selected calcareous oil shales

Sample	Major element composition									
	SiO_2	Al_2O_3	CaO	P_2O_5	SO_3	MgO	FeO	TiO_2	K_2O	Na_2O
EB-1										
a	22.7	11.0	10.4	2.6	19.7	14.3	2.9	0.0	3.7	12.8
b	23.8	10.1	27.0	1.9	8.2	18.1	7.0	0.7	0.3	2.9
EB-2										
a	32.4	16.7	11.3	2.6	10.3	6.7	4.3	1.1	1.7	13.0
b	36.8	16.0	18.5	3.6	3.9	9.0	5.8	0.9	0.7	4.9
EB-3										
a	25.8	12.3	35.1	6.6	7.6	6.0	3.0	0.6	1.2	1.9
b	23.2	11.0	39.4	3.4	3.8	12.5	5.0	0.4	0.1	1.3
EB-4										
a	25.0	10.6	35.1	5.7	7.4	8.8	3.6	0.8	1.2	1.9
b	20.1	8.5	43.4	5.0	3.5	15.6	2.9	0.6	0.0	0.5
EB-5										
a	24.7	11.7	36.7	3.6	9.4	6.4	3.7	0.5	1.4	1.9
b	20.2	8.6	40.6	2.8	5.4	16.6	4.3	0.5	0.0	1.0

(a) The composition of the raw oil shales without the amount of CO_3. (b) The composition of the decarbonated samples at 1,000 °C

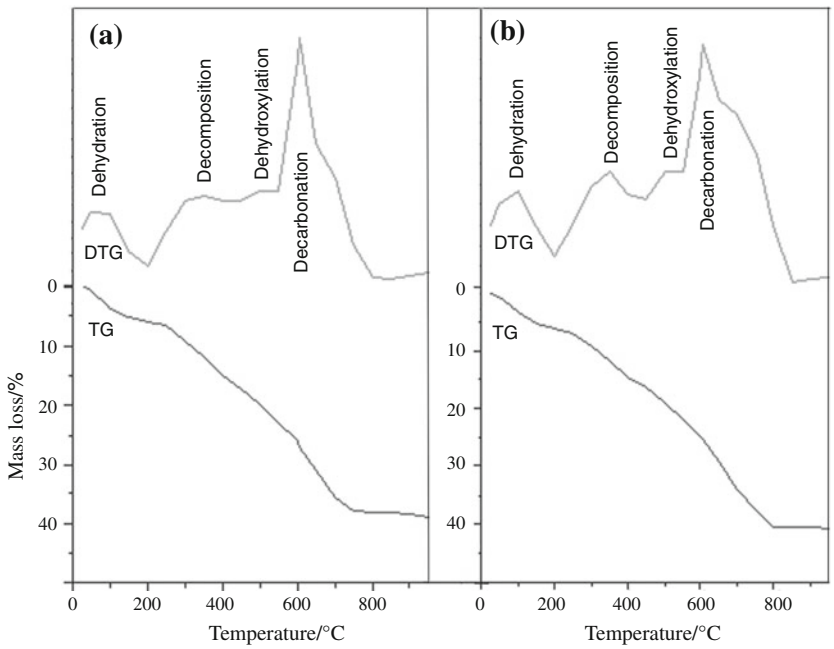

Fig. 9 Thermogravimetric TG and DTG curves of the calcareous oil shales heated up to 1,000 °C: **a** sample EB-3, and **b** sample EB-5. The peaks in the DTG curves are related to dehydration of water, decomposition of some organic matter, dehydroxylation of clay minerals, and decarbonation of carbonate minerals (calcite or dolomite)

3,640 cm^{-1} in the spectra of the rehydrated calcined oil shales is related to portlandite. An additional OH band which may relate to the hydroxylellestadite is not detected.

Several processes have been suggested for the thermal formation of the ellestadite. Yoffe et al. [7] found that this mineral is practically only in the combustion of oil shales, rich in apatite and in sulfur, and suggested that, in calcination of calcareous oil shales, ellestadite is crystallized by an epitaxial growth of the ellestadite on apatite nuclei. According to Yoffe et al. [5], during the combustion of calcareous oil shales, the SO_2 gas react with the amorphous silicates in the deposit forming hydroxylellestadite. Ellestadite is an apatite-type structure mineral [22–24] and thus it may be formed by thermal diffusion and substitution in the apatite structure. According to Knubovets et al. [25], in the calcination of phosphorite, isomorphous substitution of PO_4^{3-} by SO_4^{2-} and SiO_4^{4-} may take place in the presence of sulfur-rich organic matter and silica minerals. The SO_4^{2-} and SiO_4^{4-} enter the apatite structure in the vacant orthophosphate positions produced by the ousting of the carbonate, at 800 °C and sometimes already at 700 °C. Baumer et al. [26] argue for the occurence of a coupled

substitution ($2PO_4^{3-} \rightarrow SO_4^{2-} + SiO_4^{4-}$). It appears that, during the combustion, a thermal transformation of the apatite to ellestadite may take place. The isomorphous substitution of PO_4 by SO_4 occurred when sulfate from the decomposed organic matter enters into the apatite structure. Substitution of PO_4 by SiO_4 takes place in the presence of silica minerals (opal C-T, clays or even quartz) in the oil shales.

Dehydroxylation of the clay minerals

Dehydroxylation of the clay minerals is observed by the DTG curve (Fig. 9) and by the disappearance of their characteristic OH-stretching bands in the spectra of samples heated at 600 °C (Fig. 8c). Kaolinite and smectite dehydroxylate at about 500 and 600 °C [16] and transforms to metakaolinite and meta-smectite at higher temperatures [10, 16, 27].

The formation of gehlenite

The formation of gehlenite is already observed in the spectra and in the curve fitted spectra of samples heated above 600 °C (Figs. 4, 5, 6, 7). The presence of gehlenite at 1,000 °C is confirmed by the XRD analysis (Fig. 2). The gehlenite is formed by the thermal reaction of free lime with metakaolinite [15, 16, 28, 29].

Summary

In the combustion of calcareous oil shales a thermal sulfatization process takes place. Although there is a high sulfur concentration in the raw calcareous oil shale, because of the sulfatization process, a great part of the sulfur content of the raw oil shales is retained in the calcined ashes forming anhydrite and ellestadite and the release of sulfur gas to the atmosphere decreases. Thus, the use of calcareous oil shales for energy source has less environmental harmful than that of the clayey oil shales.

FT-IR spectroscopy and spectral analysis seems to be useful methods for phase analysis of oil shales in combustion industry. The spectroscopic analysis is advantageous in analysis of amorphous and short-range ordered thermal phases, such as metakaolinite and meta-smectite and proto-phases (at 600 °C) of gehlenite and ellestadite, which are lacking of XRD peaks. The applying of curve-fitting allows improving the identification of the individual thermal phases and to estimate their relative amounts.

Acknowledgements The support for research extended by The Open University of Israel's Research Fund (grant no. 31016), is gratefully acknowledged. The assistance of Dana Harari and Galina Kaz in the laboratory is greatly acknowledged. The language editing of Beverly Katz is also appreciated.

References

1. Dinur D, Spiro B, Aizenshtat Z. The distribution and isotopic composition of sulfur in organic rich sedimentary rocks. Chem Geol. 1980;31:37–51.
2. Yurum Y, Levy M. Quantitative determination of shale oil compounds by gas chromatography-mass spectrometry-selected ion monitoring. Fuel Process Technol. 1985;11:59–69.
3. Yefimov V, Doilov S, Pulemiotov I. Research and experimental processing of high-sulfur oil shales. Oil Shale. 1995;12:317–40.
4. Minster T, Yoffe O, Nathan Y, Flexer A. Geochemistry, mineralogy, and paleoenvironments of deposition of the Oil Shale Member in the Negev. Isr J Earth Sci. 1997;46:41–59.
5. Yoffe O, Wolfarth A, Nathan Y, Cohen S, Minster T. Oil shale fueled FBC power plant—ash deposits and fouling problems. Fuel. 2007;86:2714–27.
6. Spiro B. Geochemistry and mineralogy of bituminous rocks in Israel. Unpublished Ph.D. Thesis, Hebrew University of Jerusalem, 1980 (in Hebrew, English abstract).
7. Yoffe O, Nathan Y, Wolfarth A, Cohen S, Shoval S. The chemistry and mineralogy of the Negev oil shale ashes. Fuel. 2002;81:1101–17.
8. Heller-Kallai L, Esterson G, Aizenshtat Z, Pismen M. Mineral reactions and pyrolysis of Israeli oil shale. J Anal Appl Pyrolysis. 1984;6:375–89.
9. Maenami H, Isu N, Ishida EH, Mitsuda T. Electron microscopy and phase analysis of fly ash from pressurized fluidized bed combustion. Cem Concr Res. 2004;34:781–8.
10. Shoval S, Michaelian KH, Boudeulle M, Panczer G, Lapides I, Yariv S. Study of thermally treated Dickite by infrared and micro-Raman spectroscopy using curve-fitting technique. J Therm Anal Calorim. 2002;69:205–25.
11. Farmer VC. The Infrared spectra of minerals, monograph 4. London: Mineralogical Society; 1974.
12. Shoval S, Gaft M, Beck P, Kirsh Y. The thermal behavior of limestone and monocrystalline calcite tempers during firing and their use in ancient vessels. J Therm Anal. 1993;40:263–73.
13. Heller-Kallai L, Miloslavski I, Aizenshtat Z. Dissolution of calcite by steam derived from clay minerals. Naturwissenschaften. 1986;73:615–6.
14. Heller-Kallai L, Miloslavski I, Aizenshtat Z. Volatile products of clay mineral pyrolysis revealed by their effects on calcite. Clay Miner. 1987;22:339–48.
15. Mackenzie RC, Rahman AA. Interaction of kaolinite with calcite on heating: I. instrumental and procedural factors for one kaolinite in air and nitrogen. Thermochim Acta. 1987;121:51–69.
16. Shoval S. Mineralogical changes upon heating calcitic and dolomitic marl rocks. Thermochim Acta. 1988;135:243–52.
17. Mackenzie RC. Differential thermal analysis, vols 1, 2. London: Academic Press; 1970, 1972.
18. Matthews A, Nathan Y. The decarbonation of carbonate-fluorapatite (francolite). Am Mineral. 1977;62:565–73.
19. Spiro B. Geochemistry and mineralogy of bituminous rocks in Israel. Ph.D. Thesis, Hebrew University of Jerusalem, 1980.
20. Tullin C, Nyman G, Ghardashkhani S. Direct sulfation of $CaCO_3$: the influence of CO_2 partial pressure. Energy Fuels. 1993;7:512–9.
21. Shoval S, Yofe O, Nathan Y. Distinguishing between natural and recarbonated calcite in oil shale ashes. J Therm Anal Calorim. 2003;71:883–92.
22. Harada K, Nagashima K, Nakao K, Kato A. Hydroxylellestadite, a new apatite from Chichibu mine, Saitama Prefecture, Japan. Am Mineral. 1971;56:1507–18.

23. Rouse RC, Dunn JP. A contribution to the crystal chemistry of ellestadite and the silicate sulfate apatites. Am Mineral. 1982; 67:90–6.
24. Elliott JC. Structure and chemistry of the apatites and other calcium orthophosphates. London: Elsevier; 1994. p. 230–4.
25. Knubovets R, Nathan Y, Shoval S, Rabinowitz J. Thermal transformations in phosphorites. J Therm Anal. 1997;50:229–39.
26. Baumer A, Caruba R, Ganteaume M. Carbonate-fluorapatite: mise en evidence de la substitutions couplees 2 $PO_4 \rightarrow SiO_4 + SO_4$ par spectrometrie infrarouge. Eur J Mineral. 1990;2:297–304.
27. Heller L, Farmer VC, Mackenzie RC, Mitchell BD, Taylor HFW. The dehydroxylation and rehydroxylation of triphormic dioctahedral clay minerals. Clay Miner Bull. 1962;5:56–72.
28. Mackenzie RC, Rahman AA, Moir HM. Interaction of kaolinite with calcite on heating II. Mixtures with one kaolinite in air and nitrogen. Thermochim Acta. 1988;121:51–69.
29. Riccardi MP, Messiga B, Duminuco P. An approach to the dynamics of clay firing. Appl Clay Sci. 1999;15:393–409.